IEEE Photonics Journal
An IEEE Photonics Society Publication

Open Access

Heterogeneously Integrated InGaAs and Si Membrane Four-Color Photodetector Arrays

Volume 8, Number 2, April 2016

Laxmy Menon
Hongjun Yang, Member, IEEE
Sang June Cho
Solomon Mikael, Member, IEEE
Zhenqiang Ma, Senior Member, IEEE
Carl Reuterskiöld-Hedlund
Mattias Hammar
Weidong Zhou, Senior Member, IEEE

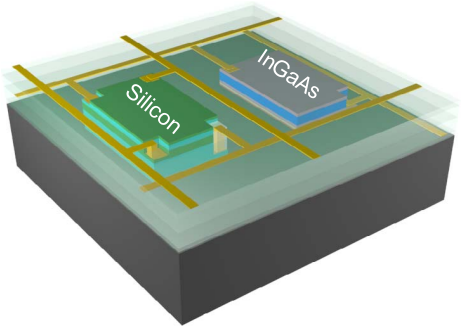

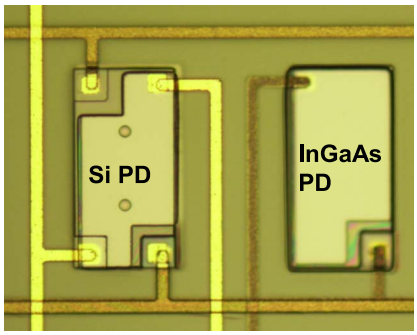

DOI: 10.1109/JPHOT.2016.2544545
1943-0655

IEEE photonics SOCIETY

IEEE

Heterogeneously Integrated InGaAs and Si Membrane Four-Color Photodetector Arrays

Laxmy Menon,[1] Hongjun Yang,[1,4] *Member, IEEE*, Sang June Cho,[2] Solomon Mikael,[2] *Member, IEEE*, Zhenqiang Ma,[2] *Senior Member, IEEE*, Carl Reuterskiöld-Hedlund,[3] Mattias Hammar,[3] and Weidong Zhou,[1] *Senior Member, IEEE*

[1]Department of Electrical Engineering, The University of Texas at Arlington, Arlington, TX 76019 USA
[2]Department of Electrical and Computer Engineering, University of Wisconsin-Madison, Madison, WI 53706 USA
[3]School of Information and Communication Technology, KTH Royal Institute of Technology, 164 40 Kista, Sweden
[4]Semerane, Inc., Arlington, TX 76010 USA

DOI: 10.1109/JPHOT.2016.2544545

Manuscript received February 22, 2016; revised March 13, 2016; accepted March 15, 2016. Date of current version April 1, 2016. This work was supported by the Air Force Office of Scientific Research under Grant FA9550-13-C-0011 (Program Manager: Dr. G. Pomrenke). Corresponding author: W. Zhou (e-mail: wzhou@uta.edu).

Abstract: We report the design and fabrication of heterogeneously integrated silicon and InGaAs membrane photodetector arrays. Visible and near-infrared (NIR) detection can be achieved by transfer printing a silicon membrane on InGaAs substrate. Based on the penetration-depth-dependent absorption of different wavelengths, filter-free visible color detection can be obtained via three-junction photocurrent measurement for silicon, and NIR can be detected by InGaAs. The measurements show good agreement with the optical behavior predicted by the design and simulation.

Index Terms: Heterogeneous, imager, near-infrared (NIR), photodetector arrays, visible.

1. Introduction

Multi-band and multispectral imaging has various applications in remote sensing, automotive, industrial surveillance systems, and the medical field. Simultaneous acquisition of visible and infrared (IR) is especially of interest, according to the recent market trends. Several approaches have been reported in literature to capture and separate visible and near-infrared (NIR) information of a scene. The main methods used currently to sense and separate visible and IR wavelengths involve 1) the use of color filter arrays (CFAs), 2) the use of external mechanical filters, and 3) the use of depth dependent absorption property of materials. Most of the approaches to detect visible and IR wavelengths fall under the first category, where a GRGB pattern of color filters is placed over the imager sensors to detect colors. The GRGB is replaced with a RGBW, where W stands for panchromatic, which is sensitive to all wavelengths [1]. Due to the large sensitivity of W pixel to visible wavelengths and the large sensitivity of the RGB cells to NIR wavelengths, this approach has issues. Some attempts have been made to rectify the errors, by using photonic crystals with defect layers to form IR blocking layers at each RGB pixel location, leaving the W pixel

unfiltered. In the second category, the two main approaches are either to capture the same scene through two separate cameras simultaneously or to use an IR blocking filter or a visible blocking filter to simultaneously take two images of the same scene. Both of these methods require lot of post processing like image fusion [2], [3], and the need to mechanically replace filters or use two cameras, which make them expensive, bulky and slow. In addition, more processing power is needed to analyze and compare two separate images. Lyu *et al.* [4] have made a vertically integrated photodiode structure (VIPS) which utilizes the method in the third category. Here, a deep buried photodiode was formed beneath the normal RGB photodiodes, to absorb and detect the NIR wavelength, while the color filters on top for R, G, and B selection, detect visible radiation, similar to a CFA. Since the area of the deep photodiode and the R, G, B pixels are different, the resolution of IR images will be quarter of that of visible images. Langfelder [5] proposed a topology to detect visible and IR radiation, based on the principle of Transverse Field detector, which also relies on the absorption properties of radiation in silicon. Here, by suitable biasing of the collecting junctions on the surface, the charge carriers generated at different depths can be collected by means of transverse electric fields. Martin *et al.* [6] reported a Visible InGaAs Focal Plane Array (FPA), where they have increased the quantum efficiency of InGaAs in the visible band, by removing or thinning the InP substrate, which is responsible for absorbing most of the visible light in a back illuminated structure.

The method used in this paper falls into the third category. In semiconductor materials, the absorption depth of photons varies with the energy of photons. This property can be utilized to build a multicolor detector, using silicon, by having several PN junctions stacked on top of each other, as the absorption depth of Si varies over several orders of magnitude over the visible range. By building a vertically integrated structure, we can avoid the inevitable transmission loss, color aliasing effect and resolution limitation encountered with color filter array (CFA) based sensor arrays [7]. Thus, the carriers generated at various depths due to the difference in penetration depth of the different components of visible light can be used to determine the wavelength of the incident light. Since the bandgap of silicon limits the detection of wavelengths beyond 1.1 μm, we need a different material, like InGaAs with band gap of 0.75 eV, that is capable of detecting wavelengths up to 1.68 μm, to detect NIR radiation.

Here, we present a heterogeneously integrated silicon and InGaAs photodetector array, which is capable of detecting both visible and IR light. Two different layout architectures can be considered for this purpose-vertical stacking and adjacent placement of silicon and InGaAs. While the vertical stacking offers the best possible spatial resolution, the fabrication process is much more involved due to the challenges in patterning of very thick pixels ($\sim$9 μm deep) and additional layers of planarization and passivation of polyimides for the formation of additional interconnect layers. Here, we present the fabrication process and measurement results of the latter configuration, which can have slightly reduced complications during device processing for higher yield process-critical towards larger pixel arrays, at the cost of reduced spatial resolution. The transfer printing process reported here can be applicable to both integration architectures. The silicon detector has a vertical n-p-n-p structure, capable of detecting blue, green and red colors of the visible spectrum by utilizing the wavelength dependent absorption property of silicon, while the InGaAs detector has a PIN structure with a 2 μm intrinsic (I) region, which can detect the NIR wavelengths. The principle and working of the silicon detector has already been discussed and demonstrated in an earlier paper [8]. Based on a modified transfer printing process for accurate alignment of individual pixels for further device processing, these crystalline silicon membranes based photodetector arrays are transferred onto InGaAs substrate, enabling heterogeneously integrated photodetector arrays for focal plane array imaging and sensing applications. Using this filterless approach, a single pixel is sensitive to visible and IR wavelengths, without the use of mosaics or the need for interpolation. This approach also has the advantage of capturing visible and IR radiation in a single shot, with the same resolution, while avoiding the complicated processing steps needed to deposit IR blocking filters at pixel level. Such a heterogeneous structure can be useful in various areas like bio photonics, security monitors, automotive cameras, fluorescent imaging, spectrometer on a chip, LADAR, free space optical communications, etc.

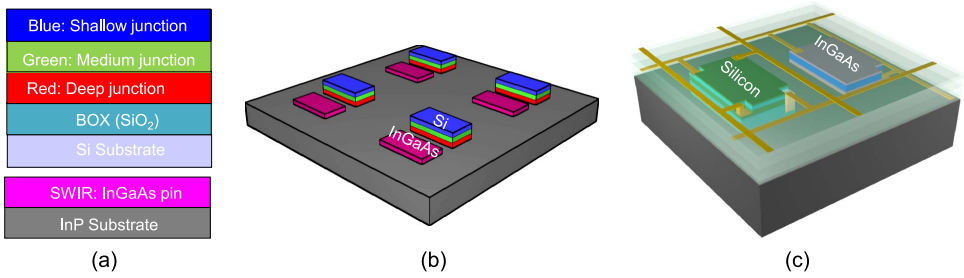

Fig. 1. Schematics of the proposed crystalline-nanomembrane-based stacked multicolor multiband photodetector arrays. (a) Three-junction SOI wafer and InGaAs single-junction wafer before transfer. (b) Si pixels transferred onto InP substrate with precise alignment with InGaAs pixel. (c) One pixel of multicolor multiband membrane imager after device completion.

2. Device Design

Based on the transfer printing process [9], we proposed and demonstrated flexible multi-color multi-band photodetector array based on crystalline silicon membranes and/or compound semiconductor membranes [8]. The schematics of the proposed heterogeneously integrated multi-color multi-band photodetector array are shown in Fig. 1. Starting with a design of triple-junction Si PDs on SOI for red (R), green (G), and blue (B) color detection [see Fig. 1(a)], the structure can be released and transfer printed onto an InGaAs substrate [see Fig. 1(b)], or stacked with other semiconductor materials for multi-band detection. One such pixel, comprising of one silicon and one InGaAs photodetector is shown in Fig. 1(c). The principle and process reported here can also be applied to a wide range of material systems, for multi-color multi-band imaging systems and spectrally resolved sensing systems for various applications. Thickness of each layer of the silicon structure optimized based on the penetration depth of blue, green and red wavelengths, and the design simulation was done using Taurus Medici software. Similarly, InGaAs PIN structure on InP substrate was designed for NIR detection. The optimized structure for Si and InGaAs is shown in Table 1. Simulated responsivities for the silicon triple junction design and the InGaAs single junction design are shown in Fig. 2. It is worth mentioning that the design optimization can lead to different responsivities for each junction for each color, with responsivities peaking for the color from the intended junction (e.g., blue junction with peak responsivity for blue color). There will be responses for other colors from each junction, as shown in Fig. 2. Algorithm will be developed to reconstruct the color information based on the different responsivities for different colors from each junction.

3. Device Fabrication

Going further with our previous transfer printing work on flexible silicon three color array [8], which was based on membrane transfer, due to the addition of InGaAs for SWIR detection in this paper, the fabrication process requires a different approach. Since the design utilizes a side by side/adjacent layout, we employed a transfer printing technique by which we can pick up the completed individual silicon mesas from the SOI substrate and transfer them adjacent to the InGaAs mesas by precise alignment. The process begins with fabricating the silicon mesas on rigid substrate by dry etching. Each corner of the mesa is used for depositing local contact pads, after etching them to the required depths for blue, green and red detection. This is followed by release-hole pattern and etching, to define holes in Si. These 8 μm diameter release holes are etched in the silicon mesa in order for HF to reach the underlying SiO_2 and etch it. HF etching was done for a short duration first to under-etch the buried oxide under the silicon mesa. This is followed by a resist coating and photolithography process, which leaves behind photoresist only in the previously under-etched areas. The SOI substrate is then immersed in HF to completely etch away the SiO_2 underneath the silicon mesas through the release holes. This separates the 6.5 μm active Si layer from the silicon handle (substrate). After this step, the

TABLE 1

Structure of (a) SOI and (b) InGaAs Used for Simulation and Fabrication

Material	Thickness	Doping	Concentration
Si	0.2 μm	n+	1E18 cm^{-3}
Si	0.4 μm	p+	1E18 cm^{-3}
Si	1.4 μm	n+	1E18 cm^{-3}
Si	4.5 μm	p+	1E18 cm^{-3}
SiO_2 1.0 μm			
Si-substrate 660 μm			

(a)

Material	Thickness	Doping	Concentration
$In_{0.53}Ga_{0.47}As$	80 nm	p	Mid E19 cm^{-3}
$In_{0.53}Ga_{0.47}As$	2000 nm	i	Low E14 cm^{-3}
$In_{0.53}Ga_{0.47}As$	400 nm	n	Low E19 cm^{-3}
InP	150 nm		UNDOPED
$In_{0.53}Ga_{0.47}As$	150 nm		UNDOPED
InP substrate			

(b)

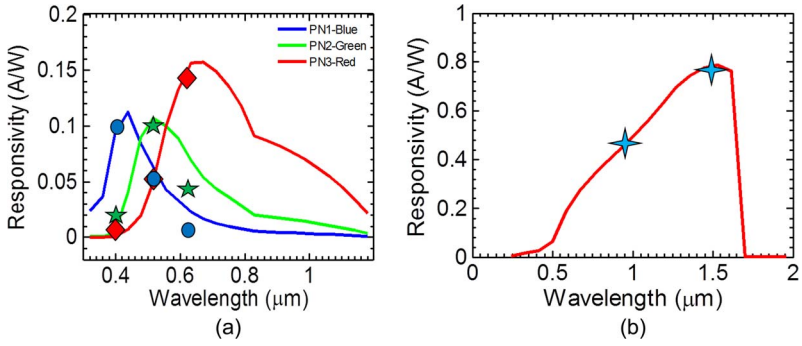

Fig. 2. Simulated (solid lines) and measured (symbols) responsivity for (a) silicon (405 nm, 532 nm, and 632 nm) and (b) InGaAs (IR–980 nm, 1550 nm).

only support for the silicon mesas is the photoresist pedestals. A PDMS stamp is used to pick up these loosely held Si mesas. Simultaneously, the InGaAs substrate is processed by defining the mesas, etching the contact areas and metal deposition to form the p and n contacts. A thin layer of SU-8 is spun on the InGaAs substrate to increase the adhesion of the Si mesas to the InGaAs substrate. Once the InGaAs is ready to receive the silicon mesas, the PDMS stamp is precisely aligned so that the silicon mesas on the PDMS can be placed adjacent to the InGaAs mesas. Once the silicon mesas are transferred to InGaAs, PDMS stamp is removed, leaving behind the Si mesas on InP substrate, aligned adjacent to the InGaAs mesas. Four interconnect layers were subsequently formed with Cr/Au for the access of individual contacts of the Si-PD pixels in the PD array. HD4104 polyimide was used as the passivation layer for the isolation of individual interconnect lines of Si and InGaAs at different depths. All the detectors have length of 100 μm and width of 200 μm, with the silicon PDs having height of 6.5 μm and InGaAs PDs with 2.56 μm. Micrographs of the fabricated device are shown in Fig. 3. Fig. 3(a) shows one pixel, which comprises of one silicon and one InGaAs photodetector. A micrograph of the 4×4 array of the heterogeneous detectors, with interconnect pads on each of the four sides, is shown in Fig. 3(b).

4. Device Characterization

Individual pixels of Si and InGaAs were first characterized, with typical results shown in Fig. 4, for the first (blue), second (green), and third (red) junctions measured under 405 nm, 532 nm, and 632 nm incident wavelengths, respectively, for silicon PD and under 980 nm and 1550 nm incident wavelengths for InGaAs PD. IV measurements were done at room temperature using a Keithley 2612 current source. The dark currents for all junctions and devices tested show less than 20 nA over reverse bias voltage up to -2 V. For the illumination measurements, light was centered on the individual devices with a lensed fiber through a light wave probe system. The

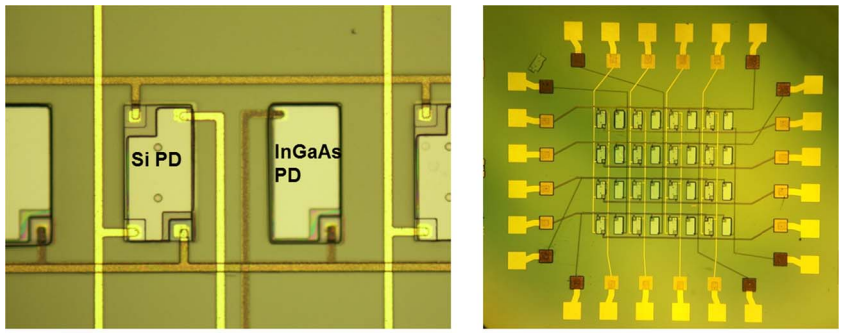

Fig. 3. Micrographs of (a) one pixel and (b) 4 × 4 array of Si/InGaAs PDs.

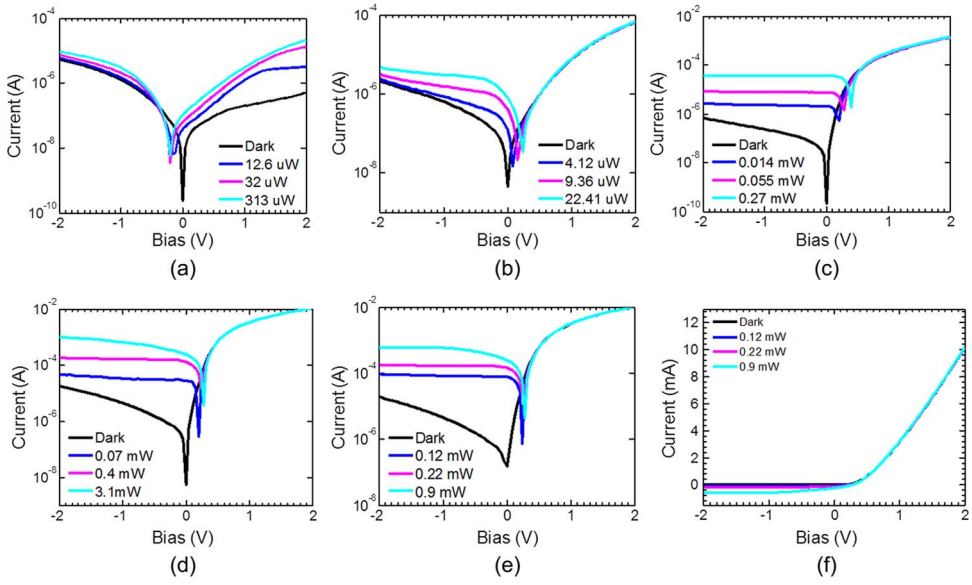

Fig. 4. Measured IV characteristics of blue, green, and red junctions of silicon under illumination with (a) 405 nm, (b) 532 nm, and (c) 632 nm and InGaAs under illumination with (d) 980-nm and (e) 1550-nm wavelengths and (f) linear graph of (e).

responses of the silicon and InGaAs detectors were measured for different input light intensities and they showed a notable increase from the dark current. The measured responsivities in silicon PD for the blue, green and red wavelengths are 0.09 A/W, 0.1 A/W, and 0.15 A/W, respectively and the measured responsivities in InGaAs PD for the 980 nm and 1550 nm wavelengths are 0.5 A/W and 0.8 A/W. All the results are shown in Fig. 2, with different symbols for the various junctions. Reasonable agreement was found between the measured values of responsivity and that predicted by simulation for the silicon photodetectors. It is to be noted that due to the contact pads placement for all three junctions in one mesa [see Fig. 3(a)], blue junction has the least amount of photosensitive area, and red junction the most. The InGaAs photodetectors had excellent agreement between the simulated and measured values of photo response. Noise Equivalent Power (NEP) and detectivity are two important figures of merit for photodetectors, and the values of these parameters for each junction at specific wavelength are shown in Table 2.

All the silicon and InGaAs detectors were tested individually for uniformity and the imaging performance was also analyzed. By measuring the spectral responsivities for each junction,

TABLE 2

NEP and Detectivity for Each Junction With the Corresponding Wavelengths

Bias (V)	NEP(W/√Hz)					Detectivity(√Hz/W)				
	405nm	532nm	632nm	980nm	1550nm	405nm	532nm	632nm	980nm	1550nm
0	7.41E-14	1.25E-14	4.51E-14	8.34E-14	1.17E-13	1.34E13	7.96E13	2.21E13	1.19E13	8.51E12
-2	8.20E-12	6.58E-12	6.80E-12	4.82E-12	3.01E-12	1.21E11	1.52E11	1.46E11	2.07E11	3.31E11

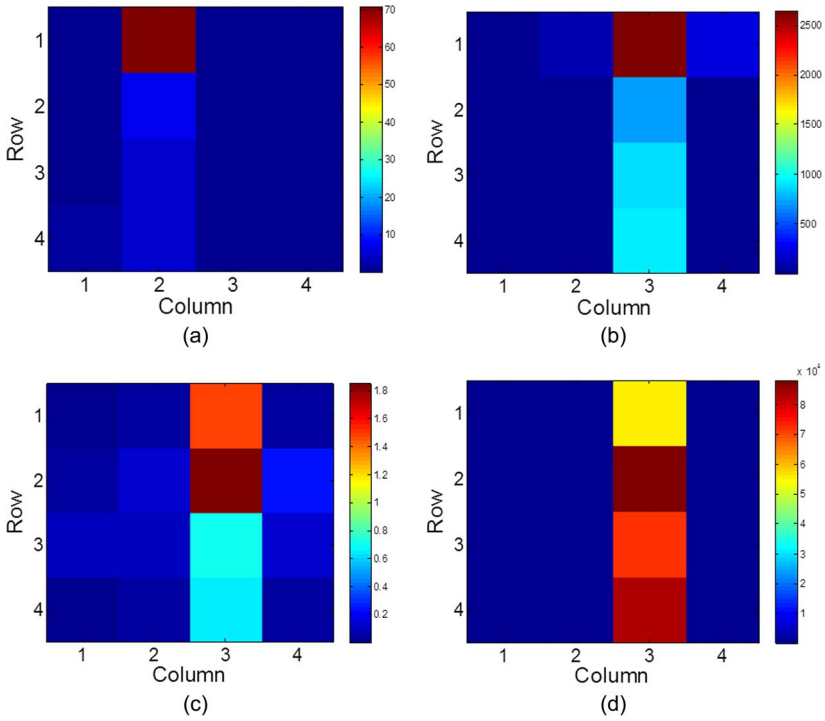

Fig. 5. Reproduced images of the illuminated column in the 4 × 4 array formed by biasing. (a) Blue junction, (b) green junction, (c) red junction, and (d) IR junction.

color (spectral) information can be resolved based on post-imaging data process, which can be used to construct color images. Imaging was done using a QTH white light source that was focused on the 4 × 4 heterogeneous photodetector array through a narrow slit, wide enough to illuminate only one column of pixels in the 4 × 4 array. On the array, the pixels that are not illuminated by the light through the slit will remain dark. The resulting photoresponse of the 16 Si (Jn1, Jn2, Jn3) photodetectors and 16 InGaAs photodetectors are recorded. The resulting image formed after data handling is shown in Fig. 5, for the blue (Jn1), green (Jn2), red (Jn3), and IR junctions. The four figures correspond to the response of Jn1, Jn2, Jn3 (For Si) and IR junction (For InGaAs) to wavelengths of 405 nm, 532 nm, 632 nm, and 1550 nm, respectively. The illuminated column (column 2 for blue junction, and column 3 for green red and IR junctions) can easily be distinguished from the non-illuminated columns. The horizontal and vertical numbers in the figures indicate the row and column number of the array. Each square in the figures represent the difference in the measured photo current and dark current for that specific junction

of the pixel. The scale bar on the right side of each figure shows the range of values in the square. Nonuniformity in color is due to the variation of this difference between the various pixels, for that specific junction, as the photoresponse of all the devices are not exactly the same. It is worth mentioning that due to the process variations, we observed better performance for the blue junctions from column 2 and better performance for other junctions from column 3. With further process optimization, we hope to obtain much better imagers with more uniform performance for all junctions/pixels. Most importantly, the junction isolation and planarization of multilayer polyimide process for multi-layer interconnects are of the major sources of process variations, which can be improved with well controlled processes for both thick photoresist patterning/alignment and patterning/curing of the multi-layer polyimide processes.

5. Conclusion

In summary, this paper demonstrated the design, fabrication, and characterization of a heterogeneously integrated Si and InGaAs photodetector array, with the ability to discriminate four colors. Each of the Si and InGaAs devices in the 4×4 array can be individually addressed. Visible and IR color information can be obtained from each detector in the array. The predictions made by simulations were verified through measurement of the fabricated array. This method of transfer printing Si photodetector on InGaAs enables us to exploit the inherent material property of Si and InGaAs to detect visible and IR radiation, without the use of external filters or CFAs. Future work will focus on obtaining higher resolution by increasing the array size, increasing fill factor, and making the heterogeneous array on a flexible platform.

Acknowledgment

The authors would like to thank IntelliEPI for providing III-V heterostructure wafers for process calibration.

References

[1] D. Hertel, H. Marechal, D. Tefera, W. Fan, and R. Hicks, "A low-cost VIS-NIR true color night vision video system based on a wide dynamic range CMOS imager," in *Proc. IEEE Intell. Veh. Symp.*, 2009, pp. 273–278.
[2] V. Tsagaris and V. Anastassopoulos, "Fusion of visible and infrared imagery for night color vision," *Displays*, vol. 26, no. 4/5, pp. 191–196, Oct. 2005.
[3] A. M. Waxman *et al.*, "Color night vision: Opponent processing in the fusion of visible and IR imagery," *Neural Netw.*, vol. 10, pp. 1–6, 1997.
[4] J.-H. Lyu, S. Choi, J. H. Choi, J. H. Nam, and J. B. Jung, "IR/color composite image sensor with VIPS (vertically integrated photodiode structure)," in *Proc. Int. Image Sens. Workshop*, 2007, pp. 7–10.
[5] G. Langfelder, "CMOS pixels directly sensitive to both visible and near-infrared radiation," *IEEE Trans. Electron Devices*, vol. 60, no. 5, pp. 1695–1700, May 2013.
[6] T. Martin, R. Brubaker, P. Dixon, M.-A. Gagliardi, and T. Sudol, "640 $\times$ 512 InGaAs focal plane array camera for visible and SWIR imaging," in *Proc. Def. Security*, 2005, pp. 12–20.
[7] D. Knipp, H. Stiebig, J. Fölsch, and H. Wagner, "Four terminal color detector for digital signal processing," *J. Non-Cryst. Solids* vol. 227, pp. 1321–1325, 1998.
[8] L. Menon *et al.*, "Transferred flexible three-color silicon membrane photodetector arrays," *IEEE Photon. J.*, vol. 7, no. 1, pp. 1–6, Feb. 2015.
[9] M. A. Meitl *et al.*, "Transfer printing by kinetic control of adhesion to an elastomeric stamp," *Nature Mat.*, vol. 5, pp. 33–38, 2005.